Chapter 5

Mathematical Model on Magnetic Drug Targeting in Microvessel

Sachin Shaw

Additional information is available at the end of the chapter

http://dx.doi.org/10.5772/intechopen.73678

Abstract

Drug targeting is a process by which the distribution of drug in an organism is deployed in such a manner that its major fraction interacts exclusively with the target tissue at the cellular or subcellular level. Magnetic drug targeting is one of the major drug delivery methods due to its noninvasiveness, high targeting efficiency, and minimized toxic side effects on healthy cells and tissues. There are several experimental works on the magnetic drug targeting through microvessel, but very few works are carried out on the mathematical models on magnetic drug delivery. The aim of the present chapter is to discuss all major and minor factors, such as fluidic force, magnetic force, particle-particle interaction, inertia force, Saffman lift force, permeability of the microvessel and carrier particle, and so on, which influenced the drug targeting through microvessel by considering the nature of blood flow as Newtonian, non-Newtonian, single phase, and two phase model. A brief details of fluidic force, magnetic force, particle-particle interaction, Saffman force, buoyancy force, etc. Mathematical models on the fluidic force are discussed for Newtonian, non-Newtonian fluid, single phase, and two-phase fluid model including other forces that influence the magnetic drug targeting in microvessel.

Keywords: magnetic drug targeting, mathematical model, non-Newtonian fluid, single phase, two-phase flow

1. Introduction

Magnetic micro- and nanoparticles are finding increasing use in different fields of microbiology, biomedicine, and biotechnology where they are used to transport and separate materials, label, and to deliver therapeutic drugs to a target tissue. The use of the magnetic particles as transport agents in different bio-applications has been discussed by Furlani [1]. They have

discussed the advantages of using magnetic nanoparticles which are well suited for the different bio-applications due to the following reasons: (1) they are nontoxic and well tolerated by living organisms after being well synthesized and functionalized; (2) they can be synthesized in sizes that range from a few nanometers to higher ranges with a very narrow interval. This nature makes them ideal for probing and manipulating bioparticles and biosystems of different ranges such as protein (5–50 nm), viruses (20–50 nm), genes (2 nm wide and 10–100 nm long), or whole cells (10–100 μm). It is also noted that sub-micron and micron-sized magnetic nanoparticles are used in different bio-applications; (3) magnetic nanoparticles are very familiar with custom-tailored surface treatment to enhance biocompatibility and enable coating with affinity biomolecules for highly specific binding with a target biomaterial; (4) magnetic nanoparticles can easily be magnetized by an applied magnetic field, but once field is removed, it reverts back to an unmagnetized state. This behavior can easily be used to separate or immobilize magnetically labeled biomaterials from a carrier fluid using an external magnetic field. Significantly, the relatively low permeability of an aqueous carrier fluid enables efficient magnet coupling to an immersed magnetically labeled biomaterial. Moreover, the low intrinsic magnetic susceptibility of most biomaterials provides substantial contrast between labeled and unlabeled material, which enables a high degree of selectivity and detection. Magnetic labeling has advantages over conventional fluorescence and chemiluminescence-based biolabels. Notably, small samples of magnetically labeled material can be detected using ultra-sensitive ferromagnetic "spin valve" sensors, which can be integrated into microfluidic-based diagnostic systems.

Magnetic particles have an additional advantage, mainly designed to absorb energy at a resonant frequency from a time-varying magnetic field, which enables their use for therapeutic hyperthermia of tumors. During radio frequency (RF) hyperthermia, magnetic nanoparticles are directed to malignant tissue and then irradiated with an AC magnetic field of sufficient magnitude and duration to heat the tissue to 42°C for 30 min or more, which is sufficient to destroy the tissue (Moroz et al., [2]). In the same manner, it will be used for other cancer therapies (Hergt and Duzt [3]; Gupta and Gupta [4]; Shaw and Murthy [5–7]). Magnetic nanoparticles are also used for bioimaging, both optically, using surface-bound fluorophores for biophotonic applications (Kircher et al. [8]; Sahoo et al. [9]; Sosnovik et al. [10]; Prasad [11]; Levy et al. [12]; Medarova et al. [13]) and magnetically where they serve as contrast agents for enhanced MRI.

Drug targeting is a process by which the distribution of drug in an organism is deployed in such a manner that its major fraction interacts exclusively with the target tissue at the cellular or subcellular level. Magnetic drug targeting is one of the major drug delivery methods due to its noninvasiveness, high targeting efficiency, and minimized toxic side effects on healthy cells and tissues (Lübbe et al. [14]; Alexiou et al. [15]). This drug targeting is mainly used for the medical treatment of various diseases, especially cancer, and cardiovascular and endovascular diseases, such as stenosis, thrombosis, aneurysm, atherosclerosis (Jurgons et al. [16]), trancheobronchial airways (Pourmehran et al. [17]), and so on. Magnetic drug targeting is a growing interest with recent progress in the development of carrier particles that are designed to target a specific tissue and effect local chemo-, radio- and gene therapy at the tumor site (**Figure 1**) (Fabrizio and Francois [18]; Berryl and Curtis [19]).

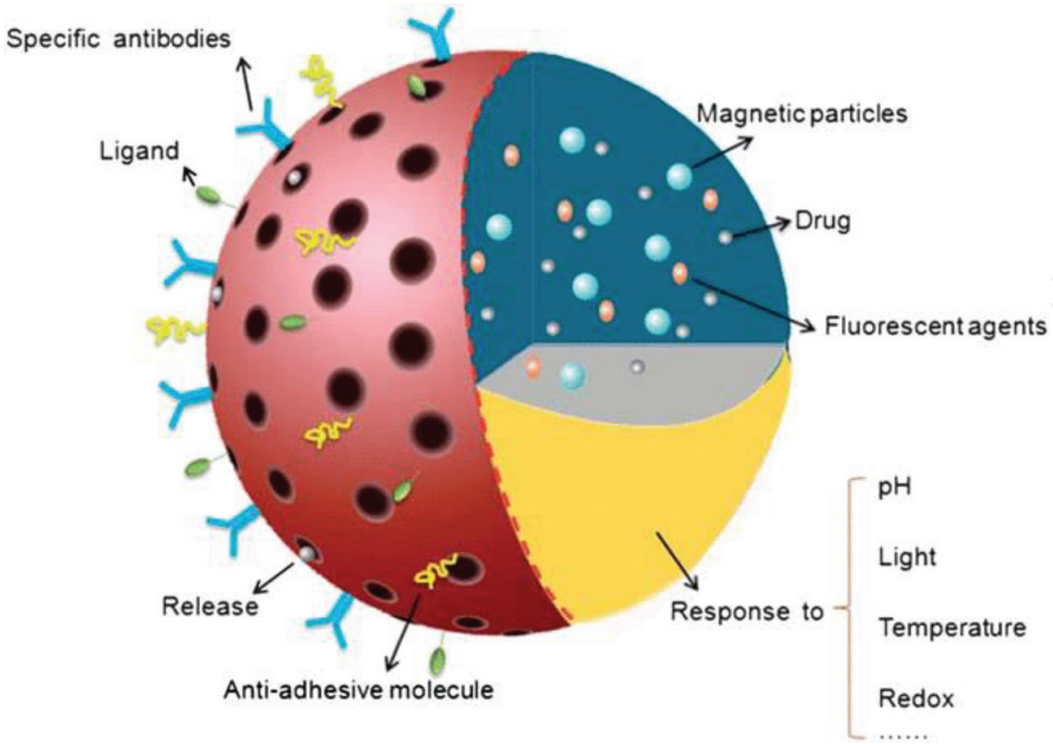

Figure 1. Schematic illustration of multifunctional and stimuli-responsive porous carrier particle, which is modified with specific antibodies, ligands targeting the cell surface, and anti-adhesive molecules (shown in the red area), and loaded with magnetic particles, fluorescent agents, and drugs for imaging, detection, and therapy (shown in the blue area). It is synthesized from stimuli-responsive polymers or modified with responsive molecules, which can respond to the change of environmental stimuli like pH, light, heat, oxides, and so on. (shown in the yellow area) (Fan et al. [20]).

Magnetic drug targeting is one of the growing interests with recent progress in the development of carrier particles that are designed to target a specific tissue to cure the tumor. In magnetic drug targeting, the therapeutic agent can be either encapsulated into a magnetic micro- or nanosphere or conjugated on its surface. Magnetic particles with bound drug molecules are injected into the vascular system upstream from the malignant tissue (**Figure 2**). They can be immobilized at the tumor site using a local magnetic field gradient produced by an external field source. Particle accumulation at the tumor is often augmented by magnetic agglomeration, and the efficiency of the accumulation depends on various physiological parameters including particle size, surface characteristics, field strength, blood flow rate, and so on (**Figure 3**).

Upon achieving a sufficient particle concentration at a tumor, drug molecules can be released from their carrier particles by changing physiological conditions such as pH, osmolality, or temperature, or by enzymatic activity (Berry and Curtis [19]; Arrueboa et al. [21]). Since the therapeutic agents are localized to regions of diseased tissue, higher dosages can be applied, which enables more effective treatment. This is in contrast to less selective conventional chemotherapy wherein a toxic drug is distributed systemically throughout the body, potentially harming healthy tissue.

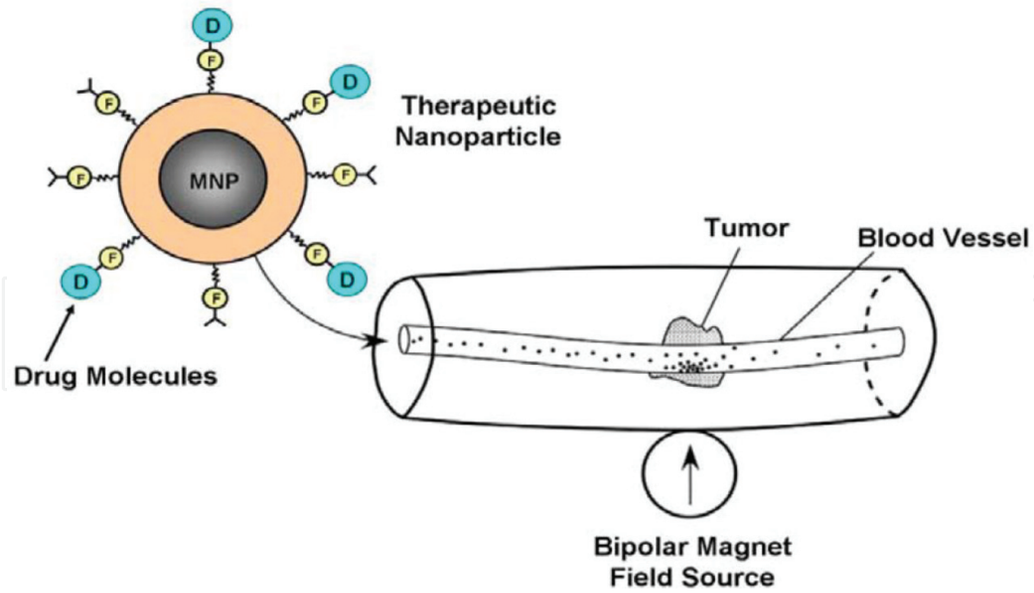

Figure 2. Noninvasive magnetic drug targeting in a microvessel (Furlani [1]).

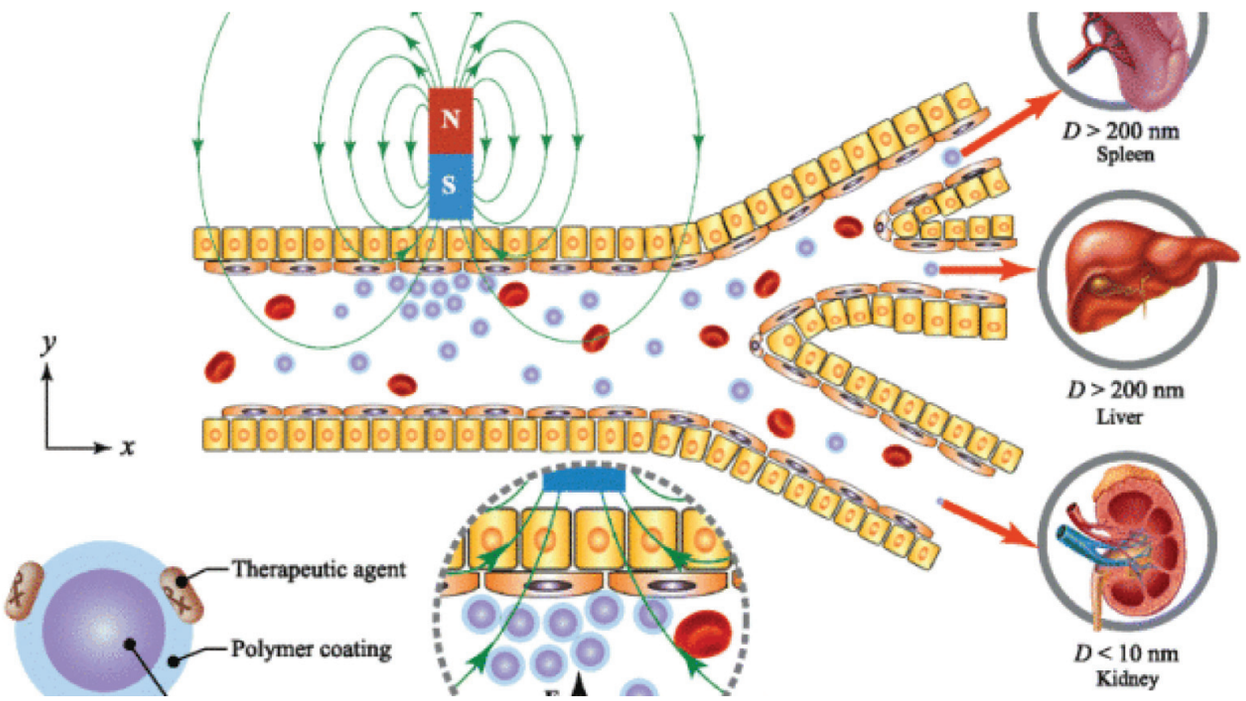

Figure 3. Drug-loaded carrier is typically composed of a magnetic core and a biocompatible coating material. The magnetic core was made from different materials such as Fe_3O_4, Fe_2O_3, or Fe. The coating materials are Au, PEG, or SiO_2. Based on the biokinetics of particles, a drug carrier ranging from 10 to 200 nm in diameter is optimal for in vivo delivery, as the small particles ($D < 10$ nm) escape by renal clearance and the large ones ($D > 200$ nm) are sequestered by the reticuloendothelial system of the spleen and liver (Lunnoo and Puangmali [22]).

During magnetic drug targeting, beyond fluidic force and magnetic force, there are several factors that play a different role in the phenomena. They are related to blood flow such as particle-particle interaction (mainly for the vessel with small radius), Saffman lift force, and so on. Some of them related to the drug particles e.g., drag force, interparticle effects such as

magnetic dipole interactions, particle-blood cell interaction, etc. Here, one by one, we discuss different forces that directly influence the trajectories of the carrier particle and on magnetic drug targeting.

2. Magnetic force on the particle

Magnetic force on the particle that flows with the fluid is well described by Furlani and Furlani [23]. By linear magnetization model, relation of magnetization and intensity of the magnetic field in the saturation can be written as

$$M_{sp} = \chi_p H_{in,\,sat}, \tag{1}$$

where $\chi_p = \mu_p/\mu_0 - 1$ is the susceptibility of the particle, μ_p is the permeability of the particle, and μ_0 is the permeability of air. The magnetic force is determined by "effective" dipole moment method as described by Jones [24] and Furlani [25]. In this method, the magnetized particle will be replaced by an "equivalent" point dipole with a moment $m_{p,\ \ eff}$, and the force on the dipole (and hence on the particle) is given by

$$F_m = \mu_f \left(m_{eff}.\nabla\right)\mathbf{H}_a, \tag{2}$$

where μ_f is the permeability of the transport fluid, m_{eff} is the effective dipole moment of the particle, and H_a is the externally applied magnetic field intensity at the center of the particle, where the equivalent dipole is located. Firstly, we solve the magneto-static boundary value problem for the particle (here the considered shape of the particle is spherical, and it may change according to the shape) immersed in a fluid where the magnetization M_p is parallel to the applied field and then determine the equivalent point dipole moment $m_{p,eff}$. Spherical coordinate system $(r.\theta,\ \ \phi)$ is considered for the spherical particle with origin as the center of the spherical particle. Cartesian coordinates (x, y, z) are considered for the microvessel and magnet (see **Figure 4**).

The potential field inside and outside of the particle can be written as

$$\Phi_{in}(r,\theta) = \nabla \mathrm{H}_{in} = -C_{in} r\cos(\theta)\left(r < R_p\right). \tag{3}$$

$$\Phi_{out}(r,\theta) = -\nabla \mathrm{H}_{out} = -H_a\, r\cos(\theta) + C_{out}\ \frac{\cos(\theta)}{r^2}\left(r \geq R_p\right). \tag{4}$$

where R_p is the radius of the spherical particle. Moreover, we considered $z-$ axis in the direction of applied magnetic field. The magnitude of the field intensity inside the particle in the $z-$ axis is

$$H_{in,z} = -\left[\frac{\partial}{\partial r}\Phi_{in}(r,\theta)\right]\cos(\theta) + \frac{1}{r}\left[\frac{\partial}{\partial r}\Phi_{in}(r,\theta)\right]\sin(\theta). \tag{5}$$

The corresponding boundary condition with respect to the potential inside and outside the particle surface and normal component of resultant of the magnetic force are written as:

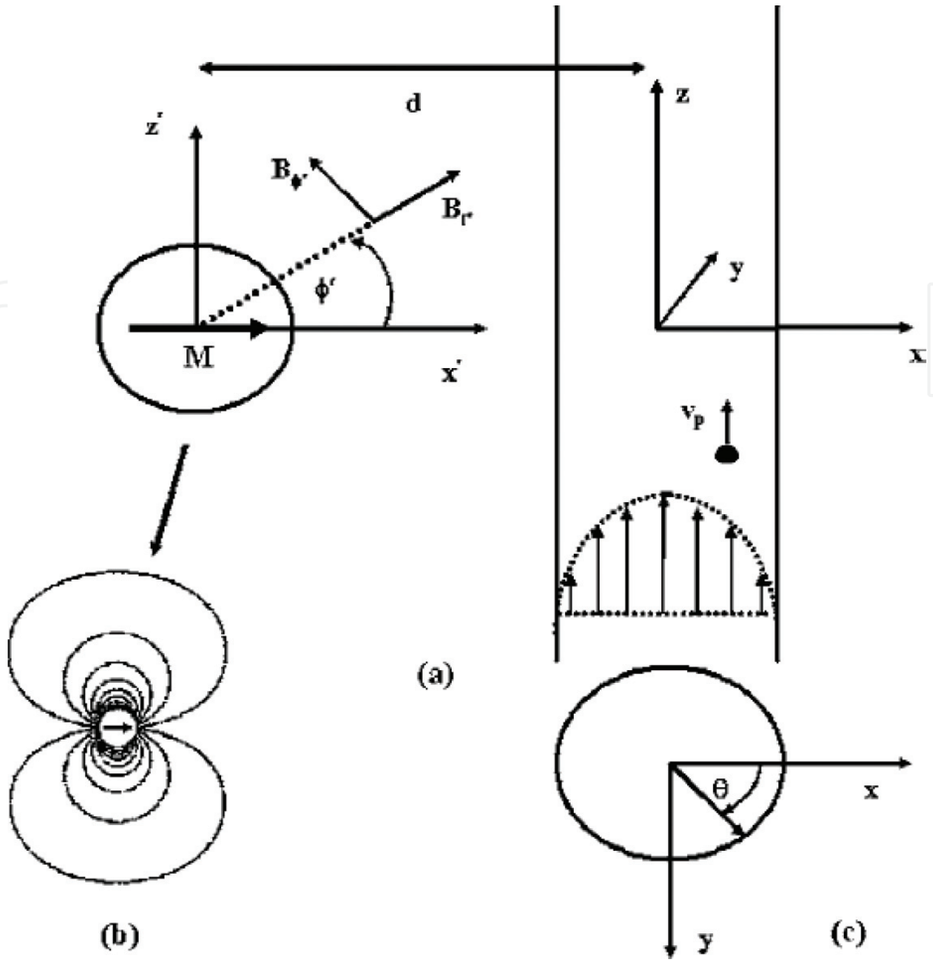

Figure 4. Geometry and reference frame for analysis: (a) coordinate systems and reference frames, (b) magnetic flux lines for a cylinder magnet, cross-section of microvessel with reference frame (Furlani [23]).

$$\begin{aligned} &\Phi_{in}(r,\theta) = \Phi_{out}(r,\theta), \\ &\mu_0\left(\frac{\partial}{\partial r}\Phi_{in} + M_p\right) = -\mu_f \frac{\partial}{\partial r}\Phi_{out}. \end{aligned} \tag{6}$$

Solving Eqs. (3) and (4) with boundary condition (6), we get

$$C_{in} = \frac{3\mu_f}{\mu_0 + 2\mu_f} H_a - \frac{\mu_0}{\mu_0 + 2\mu_f} M_a, \tag{7}$$

and

$$C_{out} = R_p^3 \left(\frac{\mu_0 - \mu_f}{\mu_0 + 2\mu_f} H_a + \frac{\mu_0}{\mu_0 + 2\mu_f} M_a \right). \tag{8}$$

From the definition (see Eq. (3)), it is clear that $H_{in} = C_{in}$ and if the particle is below the saturation, then $M_p = \chi_p H_{in}$. By substituting these two relations in Eq. (7), we get:

$$H_{in} = \frac{3\left(\chi_f + 1\right)}{\left(\chi_p - \chi_f\right) + 3\left(\chi_f + 1\right)} H_a, \tag{9}$$

and

$$M_p = \chi_p H_{in} = \frac{3\chi_p\left(\chi_f + 1\right)}{\left(\chi_p - \chi_f\right) + 3\left(\chi_f + 1\right)} H_a. \tag{10}$$

The magnitude of the "equivalent" dipole for the particle is related to C_{out}, and it can be written as

$$m_{p,eff} = 4\pi C_{out} = V_p \frac{3\left(\chi_p - \chi_f\right)}{\left(\chi_p - \chi_f\right) + 3\left(\chi_f + 1\right)} H_a, \tag{11}$$

where $V_p = (4/3)\pi R_p^3$ which is the volume of the spherical particle.

Substituting Eq. (11) into Eq. (2), we can define the magnetic force in the form of

$$F_m = \mu_f V_p \frac{3\left(\chi_p - \chi_f\right)}{\left(\chi_p - \chi_f\right) + 3\left(\chi_f + 1\right)} (\mathbf{H_a}.\nabla)\mathbf{H_a}. \tag{12}$$

Now when the susceptibility of the fluid is very small (i.e., $\left|\chi_f\right| \ll 1$), then $\mu_f \approx \mu_0$ and hence Eq. (12) can be written as

$$F_m = \mu_0 V_p \frac{3\left(\chi_p - \chi_f\right)}{\left(\chi_p - \chi_f\right) + 3\left(\chi_f + 1\right)} (\mathbf{H_a}.\nabla)\mathbf{H_a}. \tag{13}$$

In similar fashion,

$$H_{in} = \frac{3}{\left(\chi_p - \chi_f\right) + 3} H_a, \tag{14}$$

and

$$m_{p,eff} = V_p \frac{3\left(\chi_p - \chi_f\right)}{\left(\chi_p - \chi_f\right) + 3} H_a. \tag{15}$$

In general, the effective dipole moment can be written as

$$m_{p,eff} = V_p f(H_a)\mathbf{H}_a, \tag{16}$$

where

$$f(H_a) = \begin{cases} \dfrac{3\left(\chi_p - \chi_f\right)}{\left(\chi_p - \chi_f\right) + 3}, & H_a < \left(\dfrac{\left(\chi_p - \chi_f\right) + 3}{3\chi_p}\right) M_{sp} \\ M_{sp}/H_a, & H_a < \left(\dfrac{\left(\chi_p - \chi_f\right) + 3}{3\chi_p}\right) M_{sp} \end{cases} \left(|\chi_f| << 1\right), \tag{17}$$

and $H_a = |\mathbf{H}_a|$.

In this analysis, we assume that the magnet is infinitely extended in the y-direction, and therefore the $y-$ component of the magnetic field and force is considered as zero.

So, the intensity of the magnetic field and magnetic force has two components along $x-$ axis and $z-$ axis. The resultant of the intensity of the magnetic field is written as

$$\mathbf{H}_a = H_{ax}(x,z)\widehat{x} + H_{az}(x,z)\widehat{z} \tag{18}$$

and similarly, the resultant of the magnetic force is written as

$$\mathbf{F}_m = F_{mx}(x,z)\widehat{x} + F_{mz}(x,z)\widehat{z}, \tag{19}$$

where

$$F_{mx}(x,z) = \mu_0 V_p f(H_a)\left[H_{ax}(x,z)\frac{\partial H_{ax}(x,z)}{\partial x} + H_{az}(x,z)\frac{\partial H_{ax}(x,z)}{\partial z}\right], \tag{20}$$

and

$$F_{mx}(x,z) = \mu_0 V_p f(H_a)\left[H_{ax}(x,z)\frac{\partial H_{az}(x,z)}{\partial x} + H_{az}(x,z)\frac{\partial H_{az}(x,z)}{\partial z}\right]. \tag{21}$$

2.1. Magnetic field and force of a cylindrical magnet

Equations (20) and (21) represent the magnetic force for a rectangular cylinder whose y-axis extends infinitely and components of the magnetic force act along $x-$ and $z-$ axis. The calculation will be different for the case of cylindrical magnet. The cylindrical coordinate system (r', ϕ') with origin as the center of the magnet is shown in **Figure 4**.

Components of the intensity of the magnetic field in cylindrical coordinates are written as

$$H_{r'}\left(r', \phi'\right) = \frac{M_s R_{mag}^2}{2r'^2}\cos(\phi'), \tag{22}$$

and

$$H_{\phi'}\left(r', \phi'\right) = \frac{M_s R_{mag}^2}{2r'^2} \sin\left(\phi'\right). \tag{23}$$

Again, the geometry of the microvessel and flow nature is considered as the Cartesian coordinate system, and so it is necessary to convert the cylindrical coordinate system into the general Cartesian coordinate systems, say (x', z'); then, the intensity of the magnetic field in the Cartesian coordinate system is written as:

$$H_{x'}\left(x', z'\right) = \frac{M_s R_{mag}^2}{2} \frac{\left(x'^2 - z'^2\right)}{\left(x'^2 + z'^2\right)^2}, \tag{24}$$

$$H_{z'}\left(x', z'\right) = \frac{M_s R_{mag}^2}{2} \frac{2x'z'}{\left(x'^2 + z'^2\right)^2}, \tag{25}$$

and the corresponding field gradients is written as:

$$\frac{\partial}{\partial x'}\left(H_{x'}\left(x', z'\right)\right) = \frac{M_s R_{mag}^2}{2} \frac{x'\left(3z'^2 - x'^2\right)}{\left(x'^2 + z'^2\right)^3}, \tag{26}$$

$$\frac{\partial}{\partial z'}\left(H_{z'}\left(x', z'\right)\right) = \frac{M_s R_{mag}^2}{2} \frac{z'\left(z'^2 - 3x'^2\right)}{\left(x'^2 + z'^2\right)^3}, \tag{27}$$

$$\frac{\partial}{\partial z'}\left(H_{x'}\left(x', z'\right)\right) = \frac{M_s R_{mag}^2}{2} \frac{z'\left(z'^2 - 3x'^2\right)}{\left(x'^2 + z'^2\right)^3}, \tag{28}$$

$$\frac{\partial}{\partial z'}\left(H_{z'}\left(x', z'\right)\right) = M_s R_{mag}^2 \frac{x'\left(x'^2 - 3z'^2\right)}{\left(x'^2 + z'^2\right)^3}. \tag{29}$$

Finally, components of the magnetic field from Eqs. (20) and (21) with the help of expression for intensity of the magnetic fields (Eqs. (26)–(29)) in a fixed Cartesian coordinate system (x, z) with respect to the microvessel are written as:

$$F_{mx}(x, z) = -\mu_0 V_p f(H_a) M_s^2 R_{mag}^4 \frac{(x + d)}{2\left[(x + d)^2 + z^2\right]^3}, \tag{30}$$

and

$$F_{mx}(x, z) = -\mu_0 V_p f(H_a) M_s^2 R_{mag}^4 \frac{z}{2\left[(x + d)^2 + z^2\right]^3}, \tag{31}$$

where d represents the distance between the axis of magnet and the carrier particle.

This magnetic force is further simplified for noninvasive magnetic drug targeting. In this procedure, the treatment takes place in such a way that there are no breaks in the skin, and there are no contacts with skin break or mucosa, or internal body cavity beyond a natural or artificial body orifice. In this case, the magnet is placed outside the body, and the distance from the magnet to blood vessel is much larger than the diameter of the blood vessel, that is, $d \gg x$. Furthermore, we used magnetite (Fe_3O_4) as a magnetic nanoparticle, which is highly biocompatible and for that the susceptibility of the magnetic particle is much larger, that is, $\chi_{mp} \gg 1$. Based on above two assumptions, the magnetic force components are simplified to:

$$F_{mx}(x,z) = -\frac{3\mu_0 V_p M_s^2 R_{mag}^4}{2\left(d^2+z^2\right)^3}, \tag{32}$$

and

$$F_{mx}(x,z) = -3\mu_0 V_p M_s^2 R_{mag}^4 \frac{z}{2\left(d^2+z^2\right)^3}, \tag{33}$$

3. Fluidic force on the particle

Fluidic force mainly represents the drug force acts on the particle and it depends on the velocity of the fluid. There are several phenomena, and studies have been carried out to understand the blood flow though artery. Blood is a marvelous fluid. Blood consists of a suspension of red blood cells (erythrocytes), white blood cells (leukocytes), and platelets in an aqueous solution (plasma). All contain different density. The plasma is a transparent, slightly yellowish fluid, and its density is about 1.035 gm/ml which can modeled as a Newtonian fluid. The red blood cells are dominant particulate matter in blood with about 40–45% by volume of the whole blood, and it plays a vital role in changing the viscosity of the blood. In general, we use the term "hematocrit" to specify the volume percentage of red cells and entrained plasma. Platelets are much smaller than red or white cells, and so it is not so significant for the nature of blood while it plays a vital role in the formation of blood clots which may severely interfere with the flow.

3.1. Fluidic force for single-phase flow (Newtonian fluid)

We start with a simple mathematical model for drag force. Here we considered blood as a Newtonian fluid. This nature of the blood flow appears mainly for vessel of radius more than 1500 μm. The flow nature is well discussed by Furlani and Furlani [23]. Using Stokes' approximation, the fluidic force for the Newtonian fluid is written as:

$$F_f = -6\pi\eta R_{cp}\left(v_{cp} - v_f\right), \tag{34}$$

where v_{cp} is the velocity of the carrier particle, v_f is the velocity of the fluid, and η is the viscosity of the fluid. First, we are interested to find the drag force for Newtonian fluid.

Assume that the blood vessel is cylindrical and the flow is laminar, fully developed, and symmetric about the axis. So, the velocity profile is function of r (along the axis), and it is written as

$$v_f(r) = 2\overline{v}_f\left(1 - \left(\frac{r}{R_v}\right)^2\right), \tag{35}$$

where $\overline{v}_f$ is the average velocity of blood flow and R_v is the radius of the blood vessel.

With the help of Eq. (34), fluidic forces along the radial and axial radial direction are written as

$$F_{fr} = -6\pi\eta R_{cp} v_{p,x}, \tag{36}$$

and

$$F_{fz} = -6\pi\eta R_{cp}\left[v_{cp,z} - 2\overline{v}_f\left(1 - \left(\frac{r}{R_v}\right)^2\right)\right]. \tag{37}$$

3.2. Fluidic force for single-phase flow (non-Newtonian fluid model)

The radius of the microvessel plays a vital role on the nature of the blood flow. It is observed that the blood behaves as a non-Newtonian fluid due to low shear stress mainly when the diameter of the vessel is less than 1300 μm. The blood in microvessel is more complex due to the irregular geometry, mechanical behavior of blood, and its cellular constituents (mainly red blood cells). It is well established that the Casson models hold satisfactory for the blood flow through microvessel of diameter 130–1300 μm, while the Herschel-Bulkley model is more suitable for the microvessel of radius 20–100 μm (Mishra et al. [26]; Prier et al. [27]; Bugliarello and Sevilla [28]; Cokelet [29]; Merrill et al. [30]).

The drag force for the Newtonian fluid is different than the non-Newtonian fluid. The drag force for the spherical particle is written as

$$C_D = C_D(Q^*) = 24X(n)/Q^*, \tag{38}$$

where dynamic parameter $Q^* = \mathrm{Re}/(1 + Bi)^2$ with Reynolds number Re and Bingham number Bi and $X(n)$ is the rheological parameter.

For Casson fluid $X(n) = 1$, while Reynolds and Bringham number is written as (Shaw et al. [31])

$$\mathrm{Re}_{Casson} = \frac{v_{cp} d_{cp} \rho}{\nu}, \mathrm{Bi}_{Casson} = \sqrt{\frac{\rho \tau_y/\nu}{v_{cp}/d_{cp}}}, \tag{39}$$

where v_{cp} and d_{cp} are the reference velocity and diameter of the carrier particle ρ and ν are the density and kinematic viscosity of the fluid.

n	$X(n)$
0.1	1.354
0.2	1.413
0.3	1.458
0.4	1.442
0.5	1.420
0.6	1.382
0.7	1.320
0.8	1.240
0.9	1.140
1.0	1.002
1.2	0.827
1.4	0.569
1.6	0.390
1.8	0.261

Table 1. Value of rheological parameter $X(n)$ for different values of n.

For Herschel-Bulkley fluid, the rheological parameter $X(n)$ is defined in **Table 1**, and it is well correlated by the following analytical expression (Renaud et al. [32])

$$X(n) = 6^{(n-1)/2}\left\{\frac{3}{n^2+n+1}\right\}^{n+1}. \tag{40}$$

The Reynolds number and Birmingham number are written as

$$\mathrm{Re}_{HB} = \frac{v_{cp}^{2-n} d_{cp}^{n} \rho}{m}, \mathrm{Bi}_{HB} = \frac{\tau_y}{m\left(v_{cp}/d_{cp}\right)^n}, \tag{41}$$

where m is the Herschel-Bulkley model parameter.

3.3. Shape of the carrier particle

The shape of the carrier particles plays a significant role in magnetic drug targeting. A variety of nonspherical shapes including ellipsoids, discs, cylinders, hemispheres, cones, and red blood cell-like bioconcave discoids have been shown to have an impact on biological processes associated with the delivery of drugs (Geng et al. [33]; Canelas et al. [34]; Doshi and Mitragotri [35]; Enayati et al. [36]). Several experimental and laboratorial scientists have worked on the shape factor of particles in transport through the phagocytosis (Champion and Mitragotri [37]), circulation half-life (Geng et al. [33]), endocytosis (Gratton et al. [38]), targeting efficiency (Sutradhar et al. [39]), subsequent intracellular transport (Yoo et al. [40]), and vasculature (Decuzzi et al. [41]). Spherical and non-spherical carrier particles plays an imperative role on the passive drug targeting and bio-distribution of particles at the vascular level (Champion et al. [37]; Decuzzi et al. [42]; Mitragotri [43]; Fox et al. [44]). An excellent review of different shapes of carrier particles in drug delivery is given by Venkataraman et al. [45] where they discuss different experimental observations in this field and point out that understanding the implications of particle shapes would accelerate the development of

next-generation drug delivery vehicles. It is noted that the shape of the magnetic nanoparticle does not change, and it is spherical in shape.

Due to the different shapes, the drag force on the carrier particle is modified as

$$C_D = C_D(Q^*) = 24k^{'}X(n)/Q^*, \tag{42}$$

where k' is the shape constant which is defined as

$$k^{'} = \begin{cases} 1, & \text{Sphere,} \\ \dfrac{\sqrt{\beta^2 - 1}}{\beta^{1/3}\ln\left(\beta + \sqrt{\beta^2 - 1}\right)}, & \text{Prolate ellipsoid,} \\ \dfrac{2\gamma}{3}\,\dfrac{1}{\ln\gamma + 0.193}, & \text{Cylinder,} \\ \dfrac{8\pi}{3}, & \text{Circular disk.} \end{cases} \tag{43}$$

The fluidic force on the carrier particle in a laminar flow is written as

$$F_f = -\frac{1}{2}\rho A_{cp} v_{cp}^2 C_D, \tag{44}$$

where A_{cp} is a reference cross-sectional area of the carrier particle.

With the help of Eq. (34), fluidic forces for the Casson fluid along the radial and axial radial direction are written as

$$F_{fr} = -12A_{cp}\eta k^{'}\left[\left(\frac{\tau_y}{\eta}\right)^{1/2} + \left(\frac{v_{cp,x}}{d_{cp}}\right)^{1/2}\right]^2, \tag{45}$$

and

$$F_{fz} = -12A_{cp}\eta k^{'}\left[\left(\frac{\tau_y}{\eta}\right)^{1/2} + \left(\frac{v_{cp,z} - \overline{v}_f}{d_{cp}}\right)^{1/2}\right]^2. \tag{46}$$

However, fluidic forces for the Herschel-Bulkley fluid along the radial and axial radial direction are written as

$$F_{fr} = -12A_{cp}X(n)k^{'}\left[\tau_y + \eta\left(\frac{v_{cp,x}}{d_{cp}}\right)^n\right], \tag{47}$$

and

$$F_{fz} = -12A_{cp}X(n)k^{'}\left[\tau_y + \eta\left(\frac{v_{cp,z} - \overline{v}_f}{d_{cp}}\right)^n\right]. \tag{48}$$

3.4. Fluidic force for two-phase flow

Due to the microscopic properties of the blood and interaction among its different particles (Blood cells, platelets) in plasma, the nature of blood flow leads a two-phase flow model with a core of rouleaux surrounded by a cell-depicted peripheral layer. Due to the translation, deformation, and rotation, RBCs accumulated near the axis of the vessel and followed a constant velocity while the plasma layer appears near the vessel wall and velocity profile follows a parabolic profile. A mathematical model for a two-phase fluid model has been discussed by Seshadri and Jaffrin [46] in which they have considered the outer layer as cell depleted, having a lower hematocrit than the core region. Later, several researchers are worked on this direction (Gupta et al. [47]; Srivastava [48]; Sankar and Lee [49]).

3.5. Glycocalyx layer and permeability of the microvessel

Permeability of the vessel is another important characteristic, which mainly influences the flow nature of the blood. Due to the wall permeability, the fluid flows laterally and across the vessel fenestrations/pores. Fluid flow through the porous medium is defined by the Darcy law and extended Darcy law or Brinkman Law. Microvessel walls consist mainly of endothelial cell. The vascular endothelium layer helps to regulate the material exchange between circulating blood and the body tissues. The mechanism of the endothelium cells modulates microvessel permeability. It is well known that the luminal surface of the vascular endothelium is lined with a glycocalyx, a layer of membrane-bound macromolecules and adsorbed plasma proteins. This glycocalyx layer is capable of reducing or restricting the plasma flow at the peripheral layer, near to the vessel wall. Moreover, the presence of the glycocalyx layer decreases the effective cross-sectional area of the vessel available for plasma and red cell motion, so that it would possibly cause an increase in flow resistance. The flow resistance highly depends on the thickness of the glycocalyx layer. The flow resistance of the glycocalyx layer is more higher for the thick layer with respect to the thin layer (Pries et al. [27]; Weinbaum et al. [50]; Sugihara-Seki and Fu [51]). It is observed that the permeability of the microvessel significantly changes from organ to organ with the location of the microvessel and is written in ascending order as brain < skin < skeletal muscle < lung < heart <gastrointestinal tract< glomerulus of kidney.

3.6. Porosity of the carrier particle

In recent years, researchers are focused on the development of porous materials as controlled drug delivery matrices due to its unique features such as stable uniform porous structure, high surface area, tunable pore sizes with narrow distribution, and well-defined surface properties (Sher et al. [52]; Shivanand and Sprockel [53]; Ahuja and Pathak [54]) (**Figure 5**). Due to these wide physical flexibilities, porous carriers have been used in pharmaceuticals for many purposes including development of novel drug delivery systems such as floating drug delivery system, sustained drug delivery system, and improvement of solubility of poorly soluble drugs (Sharma et al. [55]; Streubel et al. [56]). These materials possess larger amounts of nanopores that allow the inclusion of drugs (Wang et al. [57]). Also, these features allow them to adsorb drugs and release them in a more reproducible and predictable manner. The use of mesoporous,

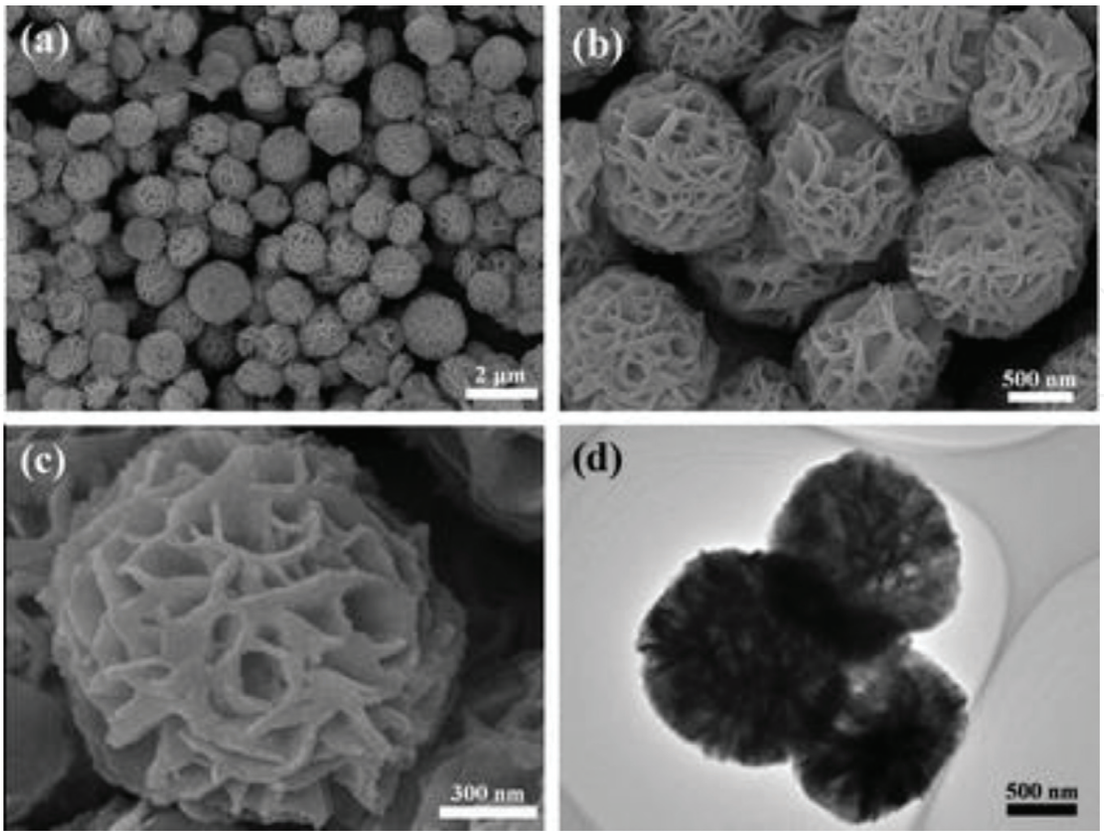

Figure 5. Electron microscopy images of porous Cu_2O nanospheres (Zhu [60]).

microporous, and nanoporous carriers for drug delivery is a part of growing research (Song et al. [58]; Andersson [59]).

4. Particle-particle interaction

In a small vessel where diameter of the vessel is less than 500 μm, it is observed that the apparent viscosity of blood is significantly decreased. This reduction of the apparent blood viscosity with decreasing diameter is continued down to the diameter of approximately 10 μm. This phenomenon was first observed by Martini et al. [61] and at the same time by Fahraeus and Lindqvist [62] during their vitro experiment to measure apparent viscosity of blood in a small narrow glass tube. This phenomenon is called as the Fahraeus-Lindqvist effect after their name. The reduction of the apparent viscosity of blood mainly appeared due to the rotation and displacement of the deformable cells (mainly red blood cells) toward the tube axis so that a cell-depleted region (mainly plasma) is formed near the wall. The effect of the cell-depleted region does not significantly influence the apparent viscosity of blood for large vessels ($d > 500$ μm) as the width of the cell-depleted layer is much smaller than the diameter of the vessel. Pries et al. [63] compiled literature data on relative blood viscosity in tube flow in vitro and obtained the empirical relationship between the relative apparent viscosity and tube diameter for red cell suspensions with a hematocrit of 45% in glass tubes.

$$\left(\frac{\mu_{app}}{\mu}\right)_{0.45} = 220e^{-1.3d} + 3.2 - 2.44e^{-0.06d^{0.645}}, \tag{49}$$

where μ_{app} is the apparent viscosity, μ is the viscosity of the plasma, and d (in μm) is the diameter of the tube. The apparent viscosity of blood for the medium-to-high flow velocities (above 50 tube diameters/s) is written as

$$\frac{\mu_{app}}{\mu} = 1 + \left[\left(\frac{\mu_{app}}{\mu}\right)_{0.45} - 1\right]\frac{(1-H_d)^C - 1}{(1-0.45)^C - 1}, \tag{50}$$

where

$$C = \left(0.8 + e^{-0.075d}\right)\left(-1 + \frac{1}{1+10(d/10)^{12}}\right) + \frac{1}{1+10(d/10)^{12}}. \tag{51}$$

Typical flow patterns of red blood cells in narrow tubes with different diameters are shown in **Figure 6**. In all cases, at the wall where the highest shear stress occurs (wall shear stress), the local viscosity of blood is the same as the viscosity of plasma ($\sim 1.2\ cP$), which reduces the wall shear stress and flow resistance.

Red blood cells are gathered near the axis of the vessel and so a cell-free region or low hematocrit region appears near the wall of the vessel. Red blood cells flow faster than the cell-depleted wall layer which mainly contains plasma and due to that the average velocity at the core region (RBCs' region) is much higher than the outer region (plasma region). This phenomenon leads to a reduction of the tube hematocrit as compared to the discharged hematocrit. A simple schematic diagram of this model is given in **Figure 6** where a steady laminar flow of suspension of cells through a tube to or from a reservoir is considered. The problem leads to conservation of mass, which is written as

$$H_T/H_d = U_S/U_C, \tag{52}$$

where H_T and H_d represent the volume concentration of cells in the tube and in reservoir, respectively. U_S and U_C are the mean velocities of the suspension and cells, respectively. In narrow tubes, $U_S < U_C$ which gives $H_T < H_d$ and it implies that H_T/H_d decreases with decrease in tube diameter. This phenomenon is called Fahraeus effect. A further decrease in tube diameter below approximate 30 μm and less, we find an increase in H_T/H_d, which known as inverse Fahraeus effect (**Figure 7**). The dependence of H_T/H_d on tube diameter D (in μm) and discharge hematocrit H_d is compiled by Pries et al. [64] and is written as

$$\frac{H_T}{H_d} = H_d + (1-H_d)\left(1 + 1.7e^{-0.415d} - 0.6e^{-0.011d}\right). \tag{53}$$

Consider a Newtonian fluid flow through the vessel as cylindrical tube of diameter d. Consider the viscosity at the core region and outside the core region (or at plasma region) as μ and μ_0, respectively. Considered the continuity of velocity and stresses at the interface of the core and

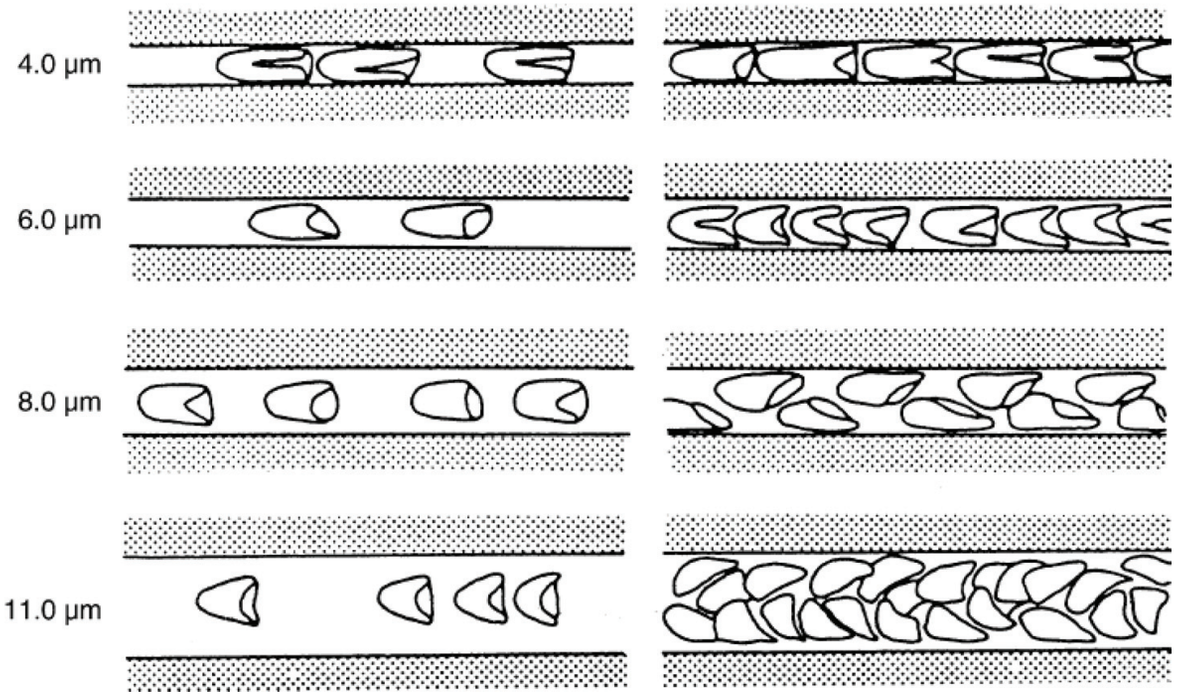

Figure 6. Schematic drawings of red cells flowing through narrow glass tubes. The flow is from right to left. The left panel is at low hematocrit, and the right panel is at high hematocrit. Single-file flow is always present in smaller tubes, whereas transition to "zipper" or multi-file flow may occur at higher hematocrit in tubes larger than approximately 7 μm (Gaehtgens [66]).

outer region while a non-slip condition on the tube of the wall. Using the abovementioned assumption, the velocity profile of the fluid as a function of radial coordinates r is written as

$$u = \begin{cases} \dfrac{P_z}{4\mu}\left[\left(\dfrac{d}{2}\right)^2 - r^2\right], & \lambda d^2 \le r \le d/2, \\ \dfrac{P_z}{4\mu_0}\left[\left(\dfrac{\lambda d}{2}\right)^2 - r^2\right] + \dfrac{P_z}{4\mu}\left(\dfrac{d}{2}\right)^2 (1-\lambda^2), & 0 \le r \le d/2, \end{cases} \tag{54}$$

where P_z represents the pressure gradient along the tube axis, λ is a constant which lies between 0 and 1, and λd is the diameter of the core region with d as the diameter of the cylinder (vessel).

Using Eqs. (52) and (53), the Fahraeus-Lindqvist effect and Fahraeus effects (Pries et al. [65]) are evaluated as

$$\mu_{app} = \frac{\mu}{1 - \left(1 - \frac{\mu}{\mu_0}\right) P_z^4}, \quad \frac{H_T}{H_d} = \frac{1}{2} \frac{1 - P_z^4\left(1 - \frac{\mu}{\mu_0}\right)}{1 - P_z^2\left(1 - \frac{\mu}{2\mu_0}\right)}. \tag{55}$$

In the limit of λ approaching 0, we have $H_T/H_d \to 1/2$ and $\mu_{app}/\mu \to 1$, and in the other way for the limit of λ approaching 1, we have $H_T/H_d \to 1$ and $\mu_{app}/\mu \to \mu_0/\mu$.

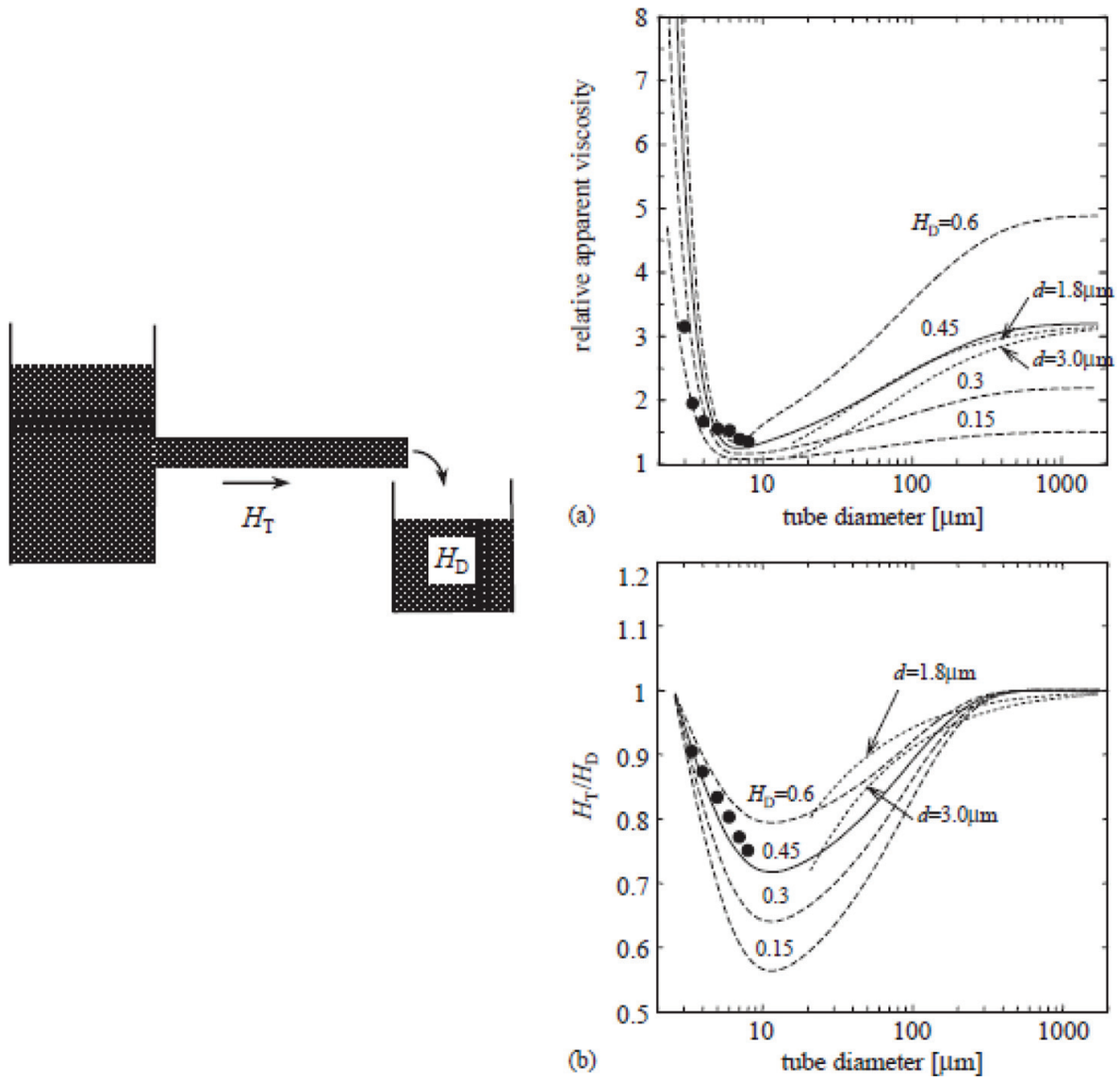

Figure 7. (a) Relative apparent viscosity of blood and (b) hematocrit ratio *HT*/*HD*, as a function of tube diameter. Solid and dashed curves, empirical fit to in vitro experimental data for blood flow in glass tubes (Eqs. (52), (53), and (55)); Dotted curves, prediction by the stacked-coins model Eq. (55); filled circles, theoretical predictions based on axisymmetric geometries at cell velocity = 1 mm/s (Secomb et al. [68]; Secomb [69]). Eqs. (52) and (55) at *HD* = 0.45 are represented by solid curves, corresponding to normal states.

4.1. Saffman lift force

Saffman lift force is mainly effective for small particles in the shear field. During drug targeting, we always used carrier particles with nanosizes, and so the particles experience a lift force perpendicular to the direction of the flow, which is known as Saffman lift force. The shear lift originates from the inertia effect in the viscous flow around the particle, and it can be defined as (Zheng and Silber-Li [67])

$$F_{saff} = 8k'\mu\sqrt{\dot{\gamma}/\nu}R_{cp}^2(v_f - v_{cp}), \tag{56}$$

where $\dot{\gamma}$ is the shear rate of the fluid and k' is the shape factor.

5. Buoyant force

For the large artery of diameter more than 1000 μm, the buoyant force plays a vital role with the convective term due to the mass of the carrier particle. The buoyant force acting on the carrier particle during its motion in the microvessel is written as

$$F_b = -V_{cp}\left(\rho_{cp} - \rho_f\right)g\mathbf{x}, \tag{57}$$

where g is the gravitational acceleration and V_{cp} is the volume of the carrier particle.

6. Geometry of the microvessel

The geometry of the microvessel is not uniform throughout the cardiovascular system. Different geometries of the vessel have been observed in the cardiovascular system, such as bifurcated vessel, with atherosclerosis inside the vessel which is attached with the wall of the vessel, curved vessel, and so on. The flow phenomenon is very complex and interesting when blood flows through curved or bifurcated or stenosed artery. Sometimes secondary flow appears near the apex of the bifurcation vessel or near stenosis. In general, numerical simulations are performed to obtain better insights into the theoretical analysis with computational fluid dynamics (Wang et al. [57]; Pourmehran et al. [17]).

7. Inertia force

Inertia force is playing an important role in blood flow through a vessel with a large diameter. In general we may use carrier particles with large radius, which can easily capture the tumor position. In general multiplication of mass of the carrier particle (which is actually same as the velocity of fluid) and acceleration of carrier particles (which is same as the acceleration of the blood flow in vessel) is not negligible, and it gives a significant influence in the magnetic drug targeting.

8. Equation of motion

Equation of the motion is followed by Newton's second law of motion. According to this law, the total force on any particle is equal to the multiplication of mass and acceleration of the particle. According to this law, the equation of motion is written as

$$m_{cp}\frac{dv_{cp}}{dt} = Sum\,of\,All\,forces = F_m + F_f + F_{saff} + F_b, \tag{58}$$

where m_{cp} is the mass of the carrier particle.

Equation (58) represents the force equation in the presence of inertia force. While in the absence of inertia force, when the diameter of the vessel is very small, then the right part of the Eq. (58) is negligible, and the equation of motion can be written as

$$0 = Sum\,of\,All\,forces = F_m + F_f + F_{saff} + F_b. \tag{59}$$

9. Conclusion and future work

Magnetic drug targeting is one of the very useful and biocompatible noninvasive methods. Still there are many scopes left to study and build different mathematical models. There are several factors that directly and indirectly act on the drug targeting and influence the trajectory of the carrier particle. Moreover, here the main focus is on the magnetic drug targeting in the cardiovascular, more particularly in the microvessel. Several experimental works have been done in this direction, which can be implemented as mathematical models. Also, magnetic drug targeting is effective for other human systems such as renal system, gastrointestinal tract, and so on.

Author details

Sachin Shaw

Address all correspondence to: shaws@biust.ac.bw

Department of Mathematics and Statistical Sciences, Botswana International University of Science and Technology, Palapye, Botswana

References

[1] Furlani EP. Magnetic biotransport: Analysis and applications. Materials. 2010;**3**:2412-2446

[2] Moroz P, Jones SK, Gray BN. Magnetically mediated hyperthermia: Current status and future directions. International Journal of Hyperthermia. 2002;**18**:267-284

[3] Hergt R, Duzt S. Magnetic parti therapycle hyperthermia-biophysical limitations of a visionary tumor. Journal of Magnetism and Magnetic Materials. 2007;**311**:187-192

[4] Gupta AK, Gupta M. Synthesis and surface engineering of iron oxide nanoparticles for biomedical applications. Biomaterials. 2005;**26**:3995-4021

[5] Shaw S, Murthy P. Magnetic drug targeting in the P ermeable blood vessel—The effect of blood rheology. Journal of Nanotechnology in Engineering and Medicine. 2010;**1**: 021001

[6] Shaw S, Murthy P, Pradhan SC. Effect of non-Newtonian characteristics of blood on magnetic targeting in the impermeable microvessel. Journal of Magnetism and Magnetic Materials. 2010;**322**:1037-1043

[7] Shaw S, Murthy P. The effect of shape factor on the magnetic targeting in the permeable microvessel with two-phase casson fluid model. Journal of Nanotechnology in Engineering and Medicine. 2011;**2**:041003 (8 Pages)

[8] Kircher MF, Mahmood U, King RS, Weissleder R, Josephon L. A multimodal nanoparticle for preoperative magnetic resonance imaging and intraoperative optical brain nanoparticle for preoperative magnetic resonance imaging and intraoperative optical brain. Cancer Research. 2003;**63**:8122-8125

[9] Sahoo Y, Goodarzi A, Swihart MT, Ohulchanskyy TY, Kaur N, Furlani EP, Prasad PN. Ferrofluid of magnetite nanoparticles: fluorescence labeling and magnetophoretic control. Journal of Physical Chemistry B. 2005;**109**:3879-3885

[10] Sosnovik DE, Nahrendorf M, Weissleder R. Magnetic nanoparticles for MR imaging: Agents, techniques and cardiovascular applications. Basic Research in Cardiology. 2008; **103**:122-130

[11] Prasad PN, Introduction to Biophotonics. NJ, USA: John Wiley & Sons: Hoboken; 2005

[12] Levy L, Sahoo Y, Kim KS, Bergey EJ, Prasad PN. Nanochemistry: Synthesis and characterization of multifunctional nanoclinics for biological applications. Chemistry of Materials. 2002;**14**:3715-3721

[13] Medarova Z, Pham W, Kim Y, Dai G, Moore A. In vivo imaging of tumor response to therapy using a dual-modality imaging strategy. International Journal of Cancer. 2006; **118**:2796-2802

[14] Lubbe AS, Alexiou C Bergenmann C. Clinical application of magnetic drug targeting, The Journal of Surgical Research;**95**(2):200-206

[15] Alexiou C, Tietze R, Schreiber E, Jurgons R, Richter H, Rahn H, Odenbach S, Lyer S. Cancer therapy with drug loaded magnetic nanoparticles—Magnetic drug targeting. Journal of Magnetism and Magnetic Materials. 2011;**323**:1404-1407

[16] Jurgons R, Seliger C, Hilpert A, Trahms L, Odenbach S, Alexiou C. Drug loaded magnetic nanoparticles for cancer therapy. Journal of Physics: Condensed Matter. 2006;**18**:S2893-S2902

[17] Pourmehran O, Gorji TB, Gorji-Bandpy M. Magnetic drug targeting through a realistic model of human tracheobronchial airways using computational fluid and particle dynamics. Biomechanics and Modeling in Mechanobiology. 2016;**15**:1355-1374

[18] Fabrizio M, Francois L. Active targeting with particulate drug carriers in tumor therapy: Fundamentals and recent progress. Drug Discovery Today. 2004;**9**:219-228

[19] Berryl CC, Curtis AS. Functionalisation of magnetic nanoparticles for appications in biomedicine. Journal of Physics D: Applied Physics. 2003;**36**:R198-R206

[20] Fan J-B, Huang C, Jiang L, Wang S. Nanoporous microspheres: From controllable synthesis to healthcare applications. Journal of Materials Chemistry B. 2013;**1**:2222-2235

[21] Arrueboa M, Fernandez-Pachecoa R, Ibarraa RM, Santamaria J. Magnetic nanoparticles for drug delivery, Nanotoday. 2017;**2**:22-32

[22] Lunnoo T, Puangmali T. Capture efficiency of biocompatible magnetic nanoparticles in arterial flow: A computer simulation for magnetic drug targeting, nanoscale research letters. 2015;**10**:426 (10 pages)

[23] Furlani EJ, Furlani EP. A model for predicting magnetic targeting of mulfunctional particles in the microvasculature. Journal of Magnetism and Magnetic Materials. 2007; **312**:187-193

[24] Jones TP. Electomagnetics of Particles. Cambridge, UK: Cambridge University Press; 1995

[25] Furlani EP. Permanent Magnet and Electomechanical Devices : Materials. Analysis and Applications, New York: Academic Press; 2001

[26] Mishra JC, Patra MK, Sahu BK. Unsteady flow of blood through narrow blood vessels—A mathematical analysis. Computers in Mathematical Application. 1992;**24**:19-31

[27] Pries AR, Secomb TW, Gaehtgens P. The endothelial surface layer. Pflügers Archiv: European Journal of Physiology. 2000;**440**:653-666

[28] Bugliarello G, Sevilla J. Velocity distribution and other characteristics of steady and pulsatile blood flow in fine glass, Biorheology. 1970;**7**:85-107

[29] Cokelet GR. The rheology of human blood: In Biomechanics, YC Fung, editor. New Jersey: Prentice Hall, Englewood Cliffs; 1972

[30] Merrill FW, Benis AM, Gilliland ER, Sherwood TK, Salzman EW. Pressure-flow relations of human blood in hollow fibers at low flow rates. Journal of Applied Physiology. 1965; **20**:954-967

[31] Shaw S, Sutradhar A, Murthy P. Permeability and stress-jump effects on magnetic drug targeting in a permeable microvessel using Darcy model. Journal of Magnetism and Magnetic Materials. 2017;**429**:227-235

[32] Renaud M, Mauret E, Chhabra RP. Power law fluid flow over a sphere: Average shear rate and drag coefficient. The Canadian Journal of Chemical Engineering. 2004;**82**:1066-1070

[33] Geng Y, Dalhaimer P, Cai S, Tsai R, Tewari M, Minko T, Discher DE. Shape effect of filaments versus spherical particles in flow and drug delivery. Nature Nanotechnology. 2007;**2**:249-255

[34] Canelas D, Herlihy KP, DeSimone JM. Top-down particle fabrication : Control of size and shape for diafnostic imaging and drug delivery. Wiley Interdisciplinary Reviews. Nanomedicine and Nanobiotechnology. 2009;**1**:391-404

[35] Doshi N, Mitragotri S. Designer biomaterials for nanomedicine. Advanced Functional Materials. 2009;**19**:3843-3854

[36] Enayati M, Ahmed Z, Stride E, Edirisinghe M. Preparation of polymeric carriers for drug delivery with different shape and size using an electric jet. Current Pharmaceutical Biotechnology. 2009;**10**:600-608

[37] Champion JA, Katare YK, Mitragotri S. Particle shape: A new design parameters for micro- and nanoscale drug delivery carriers. Journal of Controlled Release. 2007;**121**:3-9

[38] Gratton SE, Ropp PA, Pohlhaus PD, Luft JC, Madden VJ, Napier ME, Desimore JM. The effect of particle design on cellular internalization pathways. Proceedings of the National Academy of Sciences. 2008;**105**:613-618

[39] Sutradhar A, Murthy P, Shaw S. Influence of the inertia on magnetic drug targeting in microvessel-Casson model. Journal of Nanofluids. 2016;**5**:1-7

[40] Yoo J, Doshi N, Mitragotri S. Endocytosis and intracellular distribution of PGlA particles in endothelial cells: Effect of particle geometry. Macromolecular Rapid Communications. 2009;**31**:142-148

[41] Decuzzi P, Godin B, Tanaka T, Lee SY, Chiappini C, Liu X, Ferrari M. Size and shape effects in the bio-distribution of intravascularly injected particles. Journal of Controlled Release. 2010;**141**:320-327

[42] Deccuzi P, Pasqualini R, Arap W, Ferrari M. Intravascular delivery of particulate systems: Does geometry really matter? Pharmaceutical Research. 2009;**26**:235-243

[43] Mitragotri S. In drug delivery, shape does matter. Pharmaceutical Research. 2009;**26**:232-234

[44] Fox ME, Szoka FC, Frechet JM. Soluble polymer carriers for the treatment of cancer: The importance of molecular architecture. Accounts of Chemical Research. 2009;**42**:1141-1151

[45] Venkataraman S, Hedrick JL, Ong ZY, Yang C, Rachel PI, Hammond PT, Yang YY. The effects of polymeric nanostructure shape on drug delivery. Advanced Drug Delivery Reviews. 2011;**63**:1228-1246

[46] Seshadri V, Jaffrin MY. Anomalous effects in blood flow through narrow tubes: A model. INSERM-Eutomech. 1977;**92**:265-282

[47] Gupta BB, Nigam KM, Jaffrin MY. A three-layer semi-empirical model for flow of blood and other particulate suspensions through narrow tubes. Journal of Biomechanical Engineering. 1982;**104**:129-135

[48] Srivastava VP. Two-phase model of blood flow through stenosed tubes in the presence of a peripheral layer: Applications. Journal of Biomechanics. 1996;**29**:1377-1382

[49] Sankar DS, Lee U. Two-phase non-linear model for the blood flow through stenosed blood vessels. Journal of Mechanical Science and Technology. 2007;**21**:678-689

[50] Weinbaum S, Zhang X, Han Y, Vink H, Cowin SC. Mechanotransduction and flowacross the endothelial glycocalyx. PNAS. 2003;**100**:7988-7995

[51] Sugihara-Seki M, Fu BM. Blood flow and permeability in microvessels. Fluid Dynamics Research. 2005;**37**:82-132

[52] Sher P, Insavle G, Porathnam S, Pawar AP. Low density porous carrier drug adsorption and release study by response surface methodology using different solvents. International Journal of Pharmaceutics. 2007;**331**:72-83

[53] Shivananda P, Sprockel OL. A controlled porosity drug delivery system. International Journal of Pharmaceutics. 1998;**167**:83-96

[54] Ahuja G, Pathak K. Porous carriers for controlled/modulated drug delivery. Indian Journal of Pharmaceutical Sciences. 2009;**71**:500-507

[55] Sharma S, Sher P, Badve S, Atmaram PP. Adsorption of meloxicam on porous calcium silicate: Characterisation and tablet formulation. AAPS PharmSciTech. 2005;**6**:E618-E625

[56] Streubel A, Sipemann J, Bodmeier R. Floating matrix tablets based on low density foam powder: Effects of formulation and processing parameters on drug release. European Journal of Pharmaceutical Sciences. 2003;**18**:37-45

[57] Wang S, Liu H, Xu W. Hydrodynamic modelling and CFD simulation of ferrofluids flow in magnetic targeting drug delivery. International Journal of Computational Fluid Dynamics. 2008;(10):659-667

[58] Song SW, Hidajat K, Kawi S. Functionalized SAB-15 material as carrier from controlled drug delivery: Infl uence of surface properties on matrix drug interactions. Langmuir. 2005;**21**:9568-9575

[59] Andersson J, Rsenhoim J, Areva S, Linden M. Influences of material characteristics on ibuprofen drug loading and release profiles from ordered micro- and mesoporous silica matrices. Chemistry of Materials. 2004;**16**:4160-4167

[60] Zhu JJ. Nanotechweb, 19 Jan 2009 [Online] Available: http://nanotechweb.org/cws/article/lab/37301

[61] Martini P, Pierach A, Schreyer E. Die Stromung des Blutes in eigen Gefassen Eine Abweichung vom Poiseuille'schne Gesetz. Dtsch Arch Klin Med. 1930;**169**:212-222

[62] Fahraeus R, Lindqvist T. The viscosity of the blood in narrow capillary tubes. The American Journal of Physiology. 1931;**96**:562-568

[63] Pries AR, Neuhaus D, Gaehtgens P. Blood viscosity in tube flow: Dependence on diameter and hematocrit. American Journal of Physiology. 1992;**263**:H1770-H1778

[64] Prier AR, Secomb TW, Gaehtgens P. Biophysical aspects of blood flow in the microvessel. Cardiovascular Research. 1996;**32**:654-667

[65] Pries AR, Secomb TW, Gaehtgens P, Gross JF. Blood flow in microvascular networks: Experiments and simulation. Circulation Research. 1990;**67**:826-834

[66] Gaehtgens P. Flow of blood through narrow capillaries: Rheological mechanisms determining capillary hematocrit and apparent viscosity. Biorheology. 1980;**17**:183-189

[67] Zheng X, Silber-Li Z. The influence of Saffman lift force on nanoparticle concentration distribution near a wall. Applied Physics Letters. 2009;**95**:124105 (3 Pages)

[68] Secomb TW, Shalak R, Ozkaya N, Gross JF. Flow of axisymmetric red blood cells in narrow capillaries. Journal of Fluid Mechanics. 1986;**163**:405-423

[69] Secomb TW. Mechanics of Blood Flow in the Microcirculation, in Biological Fluid Dynamics. London: Company of Biologists; 1995:305-321

IntechOpen

IntechOpen